

Optical response of a single noble metal nanoparticle

Otto Muskens, Dimitris Christofilos¹, Natalia Del Fatti and Fabrice Vallée

Centre de Physique Moléculaire Optique et Hertzienne, CNRS and Université Bordeaux I, 351 cours de la Libération, 33405 Talence, France

Received 30 September 2005, accepted for publication 24 January 2006

Published 27 March 2006

Online at stacks.iop.org/JOptA/8/S264

Abstract

The characterization of a single metal nanoobject by comparing its theoretical and experimental far-field spectra measured by a spatial modulation spectroscopy (SMS) technique is discussed in the case of gold and silver nanoparticles. Quantitative determination of the polarization dependent absorption cross-section spectrum of a single nanoparticle is shown to permit its optical identification, i.e., determination of its shape, size and orientation on a surface.

Keywords: metal nanoparticles, single nanoparticle spectroscopy, nanoparticle optical properties

(Some figures in this article are in colour only in the electronic version)

1. Introduction

The novel confinement induced properties exhibited by nanoobjects and nanostructured materials are at the origin of the large interest they receive. These are directly connected to the internal characteristics (composition, structure, size, and shape) and external environment (adsorbed molecules, matrix, other particles, . . .) of the constituting nanoparticles, offering a wide range of possibilities for their modification and tailoring. In the optical domain, this sensitivity of the response is also making linear and nonlinear optical techniques very powerful characterization tools. They can be used for characterizing nanomaterials and nanoobjects [1, 2], to investigate their fundamental electronic and vibrational properties and their modifications by size reduction [3, 4], or to detect and follow the properties of nanoparticles used as labellers or as nanoprobbers of their environment [5–7].

Because of the very weak spectral- and time-domain optical response of a single nanoobject, the commonly used far-field optical techniques are usually performed simultaneously probing a large ensemble of particles, typically 10^4 – 10^6 . In realistic samples, all structural parameters fluctuate from object to object. Only averaged optical responses are observed, masking the details of the individual ones. The determination of elementary mechanisms at the

origin of the studied properties, their correlation with, for instance, the nanoparticle size, shape or environment, and their quantitative comparison with theoretical models are complex as they require the inclusion of various statistical effects. These limitations can be overcome by optically investigating single nanoparticles. This is making the development of optical techniques for detecting and characterizing single nanoobjects of central interest in both fundamental and applied nanosciences.

In this context, the high spatial resolution of near-field optical techniques is very promising, with, however, the difficulty of particle–tip coupling. For nanoobjects with strongly environment dependent optical responses, such as metal nanoparticles, complex deconvolution of the experimental data has to be performed, taking into account the characteristics of the particle and tip and of their interaction at a nanoscale [8–10]. Development of far-field spectroscopy techniques free from spurious interactions with the observation apparatus is thus of central interest. Their lower intrinsic spatial resolution can be overcome by using dilute systems so that only one particle is in the probed zone (typically a density of the order of one particle per μm^2 for two-dimensional samples). In the case of highly luminescent nanoobjects, such as semiconductor quantum dots or molecules, the detection of a single light emitter is now a routine laboratory experiment using high sensitivity photon counting and spectral selection techniques [11–13]. The observation of a single

¹ Permanent address: Division of Physics, School of Technology, Aristotle University of Thessaloniki, Thessaloniki 54006, Greece.

weakly luminescent object such as a metallic nanoparticle is more difficult since it requires the detection of other optical signatures, i.e., its absorption or scattering.

Scattering-based methods are now well established and have permitted the development of very sensitive nanoscatterer sensors [5–7]. They are limited to large nanoparticles, of typically a few tens of nanometres for standard approaches [7], and to about 5 nm using heterodyne detection [14, 15]. Scattering strongly decreasing with the particle size, as the square of their volume V , absorption that scales as V dominates the optical response of small particles. It is thus the most sensitive property to monitor for optically detecting them. A photothermal technique has recently been demonstrated based on interferometric detection of the local heating induced by single nanoparticle absorption of a laser beam [16]. However, absorption being indirectly detected, a large energy deposition in the particle is required, limiting the application of this method in spectroscopic studies. It has recently been shown that the very weak light absorption of a single nanoabsorber can be directly monitored using a spatial modulation technique permitting the detection of single gold nanospheres down to 5 nm [17]. This approach relies on spatially modulating the position of an isolated particle in the focal spot of a laser beam. It has the key advantages of requiring very low light power and of yielding quantitative information: for the first time, the absolute value of the absorption cross-section of a single nanoobject can thus be measured down to a few nm² [17]. Combining this method with a broadband supercontinuum source, the spectral and polarization dependences of the optical absorption of a single absorbing nanoparticle can be investigated. This spatial modulation spectroscopy (SMS) technique being quantitative, a full optical identification of the nanoparticle geometry (size, shape and orientation) can be performed, i.e., an ‘optical image’ of a nanoobject much smaller than the optical wavelength is obtained with a far-field technique [18]. We discuss here the principle of this optical absorption based identification in the case of gold and silver nanoparticles.

2. Optical response of a single metal nanoparticle

2.1. Nanosphere case

The optical absorption and scattering of a homogeneous metal nanosphere of diameter D embedded in an optically homogeneous matrix has been modelled by Mie [19]. The sphere and matrix materials are described via their dielectric constants, $\epsilon = \epsilon_1 + i\epsilon_2$ and ϵ_m , respectively. If the sphere is much smaller than the optical wavelength λ , keeping the lowest order terms in D/λ (dipolar approximation), the expressions of the absorption and scattering cross-sections reduce to [1, 2]

$$\begin{aligned}\sigma_a^{(s)} &= \frac{18\pi V \epsilon_m^{3/2}}{\lambda} \frac{\epsilon_2}{|\epsilon + 2\epsilon_m|^2}, \\ \sigma_s^{(s)} &= \frac{24\pi^3 V^2 \epsilon_m^2}{\lambda^4} \left| \frac{\epsilon - \epsilon_m}{\epsilon + 2\epsilon_m} \right|^2,\end{aligned}\quad (1)$$

where V is the particle volume. The same results are obtained in the quasi-static approximation [2]. In this small size approximation the extinction and absorption cross-sections

are identical, $\sigma_e^{(s)} \approx \sigma_a^{(s)}$, and much larger than $\sigma_s^{(s)}$ (for instance, $\sigma_a^{(s)}/\sigma_s^{(s)} \approx 100$ for a 20 nm gold nanosphere at its surface plasmon resonance wavelength). As is well known, confinement of the electromagnetic field leads to resonant enhancement of the nanosphere absorption (and scattering) close to the wavelength λ_R minimizing the denominator $|\epsilon + 2\epsilon_m|$, which is the condition for the surface plasmon resonance (SPR).

The SPR wavelength λ_R is determined by the particle properties, through ϵ , and by its local environment, through ϵ_m . For a small value of ϵ_2 or if it is weakly dispersed in the SPR spectral region, λ_R is determined by the simple condition [1, 20–22]

$$\epsilon_1(\lambda_R) + 2\epsilon_m = 0. \quad (2)$$

The dielectric function, ϵ , describing the metal response is modified by electron confinement in reduced dimensionality systems. In a metal, ϵ can be separated into a bound and quasi-free electron contribution:

$$\epsilon(\omega) = \epsilon_b - \frac{\omega_p^2}{\omega(\omega - i\gamma)}, \quad (3)$$

where ω_p is the plasma frequency ($\omega_p^2 = n_e e^2 / \epsilon_0 m$, n_e and m being the conduction electron density and effective mass, respectively) and γ the conduction band electron scattering rate. The response of quasi-free electrons is modified in a nanocrystal due to their interaction with the interface and the concomitant breakdown of the system periodicity. However, for metal particles larger than a few nanometres this effect is weak and can be introduced as a correction using [1, 20, 21, 23]

$$\gamma(\omega) = \gamma'(\omega) + 2gV_F/D. \quad (4)$$

The first term, γ' , takes into account bulk-like electron scattering altered by confinement in the particle [3, 24, 25]. The second term is proportional to the Fermi velocity V_F with a proportionality factor g of the order of 1 [1, 23]. Actually, to first order the electron–electron and electron–phonon scattering rates [24, 25] exhibit a $1/D$ dependence. γ' is thus also expected to vary as $1/D$, a dependence that can be lumped into the second surface effect term. In the following, the dielectric constants measured by Johnson and Christy in noble metal film [26] will be used, including a size correction with $g = 1$.

To illustrate the effects of size and environment on the SPR properties, the absorption spectra and SPR wavelength of a single gold and silver nanosphere calculated using equations (1), (3) and (4) are shown in figure 1. With increasing the matrix dielectric constant ϵ_m , the spectral position of the surface plasmon resonance shifts towards longer wavelengths (figures 1(a) and (b)). This effect is much stronger in silver than in gold, where the SPR is stabilized by the interband transitions (dispersion of ϵ_b in the SPR spectral region). In gold, these transitions that take place below about 540 nm overlap with the SPR in the 510–560 nm range, while in silver the SPR is always away from them (below 320 nm). Consequently, the SPR wavelength is very well reproduced by equation (2) in Ag (open dots in figure 1(d)), while it strongly deviates from it in Au (figure 1(c)). On the single particle level, the SPR redshift

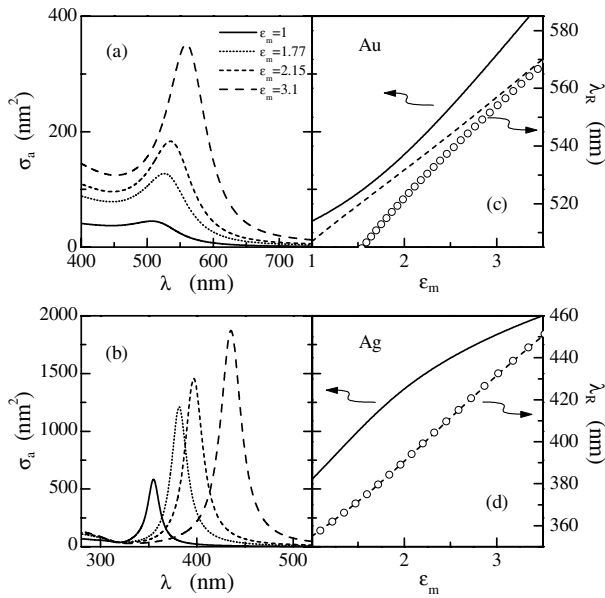


Figure 1. Computed absorption cross-section σ_a spectra around the surface plasmon resonance of a single gold (a) and silver (b) nanosphere of 15 nm diameter in vacuum ($\epsilon_m = 1$) and in different embedding matrices characterized by their dielectric constant: water ($\epsilon_m = 1.77$), fused silica ($\epsilon_m = 2.15$) and alumina ($\epsilon_m = 3.1$). Surface plasmon resonance wavelength λ_R (dashed line), and absorption cross-section at the SPR peak $\sigma_a(\lambda_R)$ (full line) for a single gold (c) and silver (d) nanosphere with $D = 15$ nm, as a function of the dielectric constant of the surrounding matrix ϵ_m . The open dots are the calculated λ_R using the approximate resonance condition equation (2).

is accompanied by a large enhancement of its absorption cross-section (figures 1(c) and (d)).

The nanoparticle size has only a weak impact on the surface plasmon resonance wavelength. In the dipolar approximation (equation (1)) it only depends on D through the size correction of ϵ (equations (3) and (4) and figure 2). Note that conversely to the prediction of the above simple model, a slight blue shift of the resonance is observed for small sizes (D smaller than about 2 nm due to quantum effects not introduced here [27]). In contrast, the peak absorption cross-section $\sigma_a(\lambda_R)$ exhibits a large size dependence, being almost proportional to the nanosphere volume (figure 2). A smaller variation is observed for small sizes due to SPR broadening induced by the size dependence of ϵ (equations (3) and (4)). To check the size-range validity of the dipolar approximation, the spectrum of a single gold or silver nanosphere has been computed using a multipolar expansion of the Mie theory up to the 11th order. The results show a deviation of the computed surface plasmon resonance wavelength for nanospheres larger than typically 20–30 nm, limiting the applicability of the dipolar model to smaller sizes (figure 2).

This analysis shows that for a given particle size in a few to few tens of nanometres range, the spectral position λ_R of the SPR and the σ_a spectrum are related (this approach is also valid for larger particles providing that fitting is performed using multipolar expansion of the Mie theory to the correct order). Actually, assuming that ϵ is well reproduced by the size corrected bulk value, the overall spectral shape of σ_a is imposed

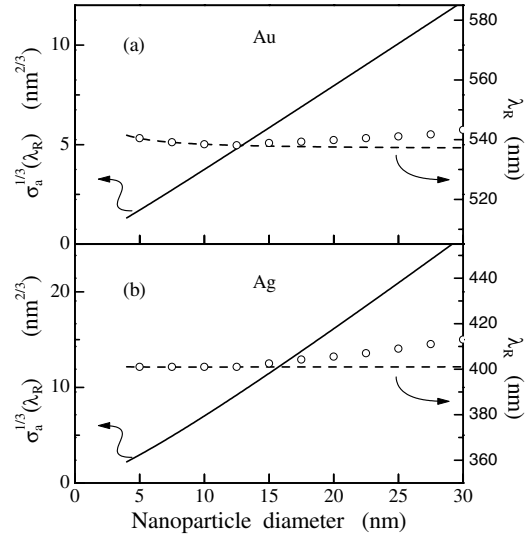


Figure 2. Size dependences of the surface plasmon resonance wavelength λ_R (dashed line), and cubic root of the absorption cross section $\sigma_a(\lambda_R)$ (full line) for a gold (a) and silver (b) nanosphere embedded in glass ($\epsilon_m = 2.25$) computed in the dipolar approximation, equation (1), using the size corrected metal dielectric function ϵ , equations (3) and (4) (see text). The open dots are the λ_R values calculated using multipolar expansion of the Mie theory up to the 11th order.

by ϵ with the only remaining parameter being ϵ_m . In particular, λ_R only depends on ϵ_m , making possible its quantitative local determination around the considered particle [28]. In contrast the absolute σ_a value is proportional to the particle volume and is thus very sensitive to its variation, permitting its precise determination. This will be experimentally exploited and confirmed in section 4.

2.2. Nanoellipsoid case

Even in good quality samples, nanoparticles frequently deviate from nanospheres. This modifies the above spectral description introducing light polarization dependent effects when a single particle is studied [1, 2]. To analyse the impact of the shape distortion, we have assumed that the particle takes an ellipsoidal shape and that its size is sufficiently small to use the quasi-static approximation [2]. In the case of a nanoellipsoid, the lower symmetry lifts the SPR degeneracy. Three surface plasmon resonances are thus observed, associated to light polarization along the ellipsoid main axes x , y and z , of full length a , b and c , respectively. For light polarized along the i direction parallel to x , y or z , the particle absorption cross section $\sigma_a^{(e),i}$ is given by

$$\sigma_{\text{abs}}^{(e),i} = \frac{2\pi V \epsilon_m^{3/2}}{\lambda L_i^2} \frac{\epsilon_2}{|\epsilon + \frac{1-L_i}{L_i} \epsilon_m|^2}. \quad (5)$$

L_i is a direction dependent geometrical factor determined by the ellipsoid shape (for a spherical particle $L_i = 1/3$). As for a sphere, for a given i polarization the SPR wavelength $\lambda_R^{(i)}$ is determined by the dielectric constant of the particle material and matrix.

As a first approximation, the size dependence of ϵ has been introduced using the sphere expression, equations (3)

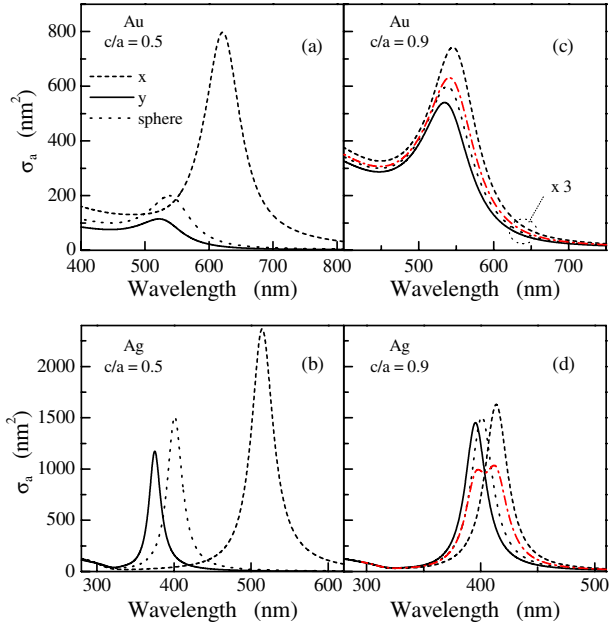


Figure 3. Computed absorption cross-section σ_a spectra around the surface plasmon resonances of a single gold prolate spheroid with $\eta = c/a = 0.5$ (a) and 0.9 (c) embedded in glass ($\epsilon_m = 2.25$) for light polarized along its long axis x and one of its short axes, y . The dotted line is the corresponding spectrum for a nanosphere of diameter $D = 15$ nm (all particles are of same volume: $D = \eta^{2/3}a$). (b) and (d): same as (a) and (c) for a silver prolate spheroid. The dashed-dotted lines in (c) and (d) are the computed spectra for unpolarized light incident perpendicular to a plane containing the long axis of the ellipsoid.

and (4), D being the diameter of a sphere of identical volume. Actually, the correction being small for the studied particle sizes and as they exhibit small deviations from sphericity (see section 4), the introduced error is negligible (a better approximation would use a size dependence given by the particle surface over volume ratio). Similarly to the sphere case, for a small or weakly dispersed $\epsilon_2(\lambda_R)$ the resonance condition reduces to

$$\epsilon_1(\lambda_R) + \frac{1 - L_i}{L_i} \epsilon_m = 0. \quad (6)$$

A special class of ellipsoidal particles are spheroids, which have two axes of equal length and thus only two distinct SPRs. For a prolate spheroid the short axes are identical: $a > b = c$, while for an oblate spheroid it is the long axes: $a = b > c$. For these shapes, analytical expressions of the geometrical factors have been derived [2]. For the long axis direction x of a prolate spheroid, it reads

$$L_x = \frac{1 - e^2}{e^2} \left(-1 + \frac{1}{2e} \ln \frac{1 + e}{1 - e} \right), \quad (7)$$

and for an oblate spheroid,

$$L_x = \frac{(1 - e^2)^{1/2}}{2e^3} \left[\frac{\pi}{2} - \arctan \left(\frac{(1 - e^2)^{1/2}}{e} \right) \right] - \frac{1 - e^2}{2e^2} \quad (8)$$

where $e^2 = 1 - \eta^2$ is the eccentricity, expressed in the particle aspect ratio $\eta = c/a$. The expressions of the other geometrical

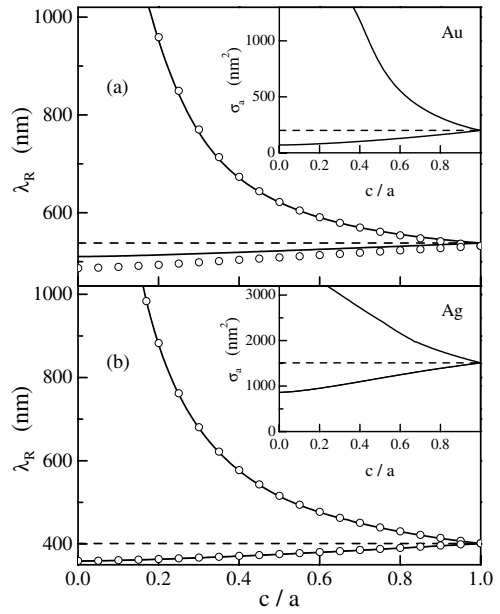


Figure 4. Computed wavelength λ_R of long and short axes (or red and blue shifted) surface plasmon resonances (full lines) of a single gold (a) and silver (b) prolate spheroid embedded in glass ($\epsilon_m = 2.25$), as a function of its aspect ratio $\eta = c/a$. The dashed line shows λ_R for a nanosphere. The open dots are the calculated λ_R using the approximate resonance condition equation (6). The insets show the corresponding absorption cross-section $\sigma_a(\lambda_R)$ for the two SPRs.

factors are given by $L_y = L_z = (1 - L_x)/2 > 1/3 > L_x$ and $L_z = (1 - 2L_x) > 1/3 > L_x = L_y$ for prolate and oblate shapes, respectively. Consequently, for the same environment defined by ϵ_m , the SPR for light polarization along the short axis is blue shifted, and it is red shifted for the long axis, as compared to the sphere case (figures 3(a) and (b)). As for the sphere case, the SPR wavelength is well predicted by equation (6) when the SPR is away from the interband transitions (open dots in figure 4). A concomitant large increase (decrease) of the amplitude of the red (blue) shifted SPR is predicted as shown in figure 4 (the same ellipsoid and sphere volumes have been assumed).

Actually, for a constant particle volume and a given polarization along one of the spheroid axes, a change of the particle shape produces a change of λ_R similar to that induced by changing the matrix refractive index (equation (5)). Non-sphericity thus clearly influences the interpretation of the measured optical spectra, and in particular, the accuracy with which the environmental parameters can be determined using near-spherical particles as nanosensors. However, even for small aspect ratio η , the anisotropy of a particle can be identified by measuring its absorption spectrum as a function of the polarization direction of a linearly polarized incident light beam. Assuming a spheroidal shape, correlated extrema of the λ_R and σ_a values are expected to show up for perpendicular polarization directions, permitting one to determine η . This is illustrated in the case of a prolate gold and silver spheroid for $\eta = 0.9$ (figures 3(c) and (d)) and will be experimentally used in section 4.

For non-polarized light, the two SPRs show up in the absorption spectra of a single nanospheroid, with amplitudes

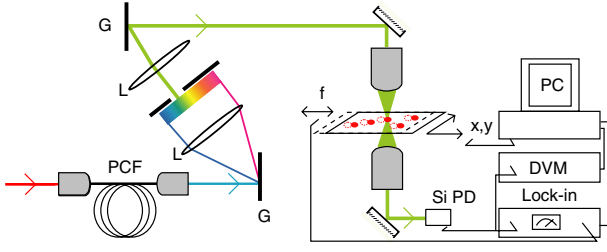


Figure 5. Single particle space modulation spectroscopy setup. The space modulation microscope is shown on the right part of the figure, with the two $\times 100$ microscope objectives and the acquisition system (a silicon photodiode (PD), lock-in amplifier, digital voltmeter (DVM) and personal computer). The sample position is modulated along the y direction at the frequency f by a piezo-electric element and displaced by a x, y piezo-scanner. The light source for gold experiments is created by injecting femtosecond pulses in a photonic crystal fibre (PCF), dispersing the created supercontinuum in a grating pair system (G), the part of the supercontinuum selected by a slit being injected in the transmission microscope.

depending on the beam direction of propagation relative to its main axes. Assuming that it propagates perpendicularly to a plane containing the long axis of a prolate spheroid, the absorption spectrum is obtained by averaging the polarized ones. In the case of gold, if the particle shape weakly deviates from sphericity, the SPR splitting reflects in a small apparent broadening of the SPR accompanied by a weak frequency shift as compared to the case of a nanosphere of identical volume (figure 3(c) for $\eta = 0.9$). In the case of silver, the larger λ_R dependence on η and the narrower resonances (due to the smaller $\epsilon_2(\lambda_R)$ value as compared to gold), lead to a strong SPR apparent broadening and a still observable double peak structure (figure 3(d)).

3. Spatial modulation spectroscopy (SMS)

The absorption cross-sections of a single 20 nm gold nanosphere is of the order of $\sigma_a \approx 100\text{--}500 \text{ nm}^2$ (figure 2(a)). The fraction of absorbed energy for a laser beam focused close to the diffraction limit can thus be estimated to be of the order of 10^{-3} . This is beyond the sensitivity limit of conventional absorption spectroscopic techniques, but can be readily detected using lock-in detection methods, provided that this absorbed fraction is modulated. It has been shown that this can be done by spatially modulating the particle position in the focal plane of the laser beam, which results in a modulation of the transmitted laser power P_t , i.e., of the sample transmission [17]. The principle of this spatial modulation microscopy technique is shown in figure 5.

For a laser beam of power P_i incident on a small particle, i.e., of size much smaller than the focal spot diameter, localized at point (x, y) on a surface perpendicular to the beam propagation direction, the total transmitted power is given by

$$P_t = P_i - \sigma_e I(x, y), \quad (9)$$

where $I(x, y)$ is the intensity spatial profile at the focal spot. In the following, $I(x, y)$ is assumed to be Gaussian with a full-width-at-half-maximum d_{FWHM} . For modulation of the particle position at a frequency f along the y direction, with an

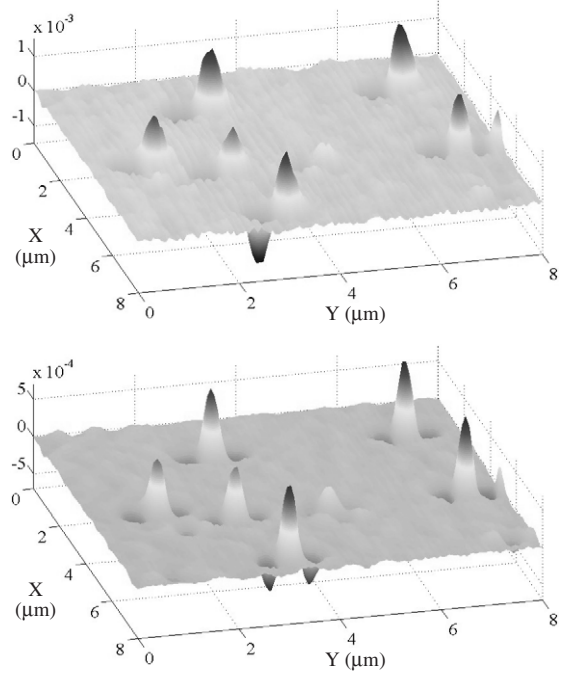


Figure 6. Images of the surface sample over an $8 \times 8 \mu\text{m}^2$ area taken using the space modulation microscope with sample position modulation at $f = 1.5 \text{ kHz}$ and signal detection at f (top) and $2f$ (bottom). The sample was prepared by spin coating a colloidal solution of gold nanoparticles with mean diameter 20 nm in the presence of PVOH. Each double (top) or triple (bottom) peak corresponds to one single nanoparticle.

amplitude δ_y much smaller than the beam size, an approximate expression can be obtained by replacing y by $y + \delta_y \sin(2\pi ft)$ in equation (9), and expanding P_t up to the second order in δ_y :

$$P_t \approx P_i - \sigma_e I(x, y) - \sigma_e \delta_y \left. \frac{\partial I}{\partial y} \right|_{(x,y)} \times \sin(2\pi ft) - \frac{1}{2} \sigma_e \delta_y^2 \left. \frac{\partial^2 I}{\partial y^2} \right|_{(x,y)} \sin^2(2\pi ft). \quad (10)$$

When recovering the modulated transmission at the fundamental, f , or harmonic, $2f$, frequency, while scanning the sample position, one obtains a sample image in which each particle yields a signal proportional to the first or second derivatives of $I(x, y)$, respectively (figure 6). For larger modulation amplitudes δ_y , the above expansion cannot be performed and the transmitted power has to be calculated numerically [29]. The above main features are retained with a maximal power transmission change obtained for $\delta_y \approx 0.85 d_{\text{FWHM}}$ for detection at f and $\delta_y \approx d_{\text{FWHM}}$ for detection at $2f$. It has been previously shown that quantitative analysis of the experimentally measured f or $2f$ component of the power transmission change $\Delta T/T = (P_i - P_t)/P_i$ yields the absolute value of the single particle absorption cross section $\sigma_e \approx \sigma_a$ [17]. Gold nanoparticles with diameters down to 5 nm were thus detected and their absorption cross-sections were found to be proportional to the particle volume in the 5–20 nm range, in agreement with the Mie theory (equation (1)).

Combining the above modulation microscopy system with a tunable light source, single nanoparticle absorption spectra

can be measured. As absorption is directly detected, only a low intensity light source with power in the μW range is required. Our experimental setup is shown in figure 5. In the case of gold particles whose SPR is around 530 nm, the spectrally broad source is provided by the white-light supercontinuum generated by nonlinear frequency broadening of the pulses delivered by a femtosecond oscillator in a photonic crystal fibre. This source has been chosen for its excellent optical properties and for its broad accessible spectral window in the visible range down to about 450 nm. In our experimental system, the 20 fs pulses produced by a homemade Ti:sapphire oscillator are injected into the fibre and a small part of the spectrum (of 2–5 nm spectral width) is selected using a double grating system and injected in our space modulation microscope. In the case of silver, whose plasmon resonance is in the blue part of the spectrum (figure 1), tunable blue light has been created by frequency doubling in a BBO crystal the femtosecond pulses delivered by the tunable Ti:sapphire oscillator.

The incident light is focused to a spot of a few hundred nanometres in diameter on the sample surface using a long working distance $100\times$ microscope objective (NA 0.8). Using the supercontinuum, the spot size ($d_{\text{FWHM}} \approx 0.7\lambda$) differs slightly from the calculated diffraction limit of 0.64λ for the microscope objective due to the limited spatial coherence of the white-light supercontinuum and to chromatic aberrations of the optical elements in the beam path (figure 5). The sample position is periodically modulated in the y direction perpendicular to the beam propagation direction, at a frequency of 1.5 kHz, by means of a piezoelectric element. The transmitted light is collected with an identical objective and detected by a silicon photodiode. The modulated part of the transmission ΔT is extracted using a lock-in amplifier and the total sample transmission T simultaneously detected using a calibrated digital voltmeter, yielding the relative change $\Delta T/T$ (figure 5). The sample is mounted onto a x – y piezoelectric translation stage permitting one to record two-dimensional images of its surface over a maximum range of $50 \times 50 \mu\text{m}^2$. The sensitivity of this setup is of the order of 10^{-5} for $\Delta T/T$ measurements. Using the calibrated d_{FWHM} and δ_y value, the wavelength dependence of the proportionality factors linking the maximum $|\Delta T/T|$ amplitude to σ_a for f or $2f$ detection can be determined, permitting precise quantitative determination of σ_a .

The samples were prepared from gold or silver colloidal solutions characterized by transmission electron microscopy (TEM). The colloidal solution was spin-coated on a glass substrate with or without polymer (polyvinyl alcohol, PVOH). By properly controlling the dilution of the initial solution, a surface density of less than one nanoparticle per μm^2 is achieved.

4. Single particle spectroscopy

An image of the sample surface spin-coated with gold nanoparticles at low density is shown in figure 6. Six isolated nanoparticles are detected over an $8 \times 8 \mu\text{m}^2$ area, with double and triple peak signatures for f and $2f$ detection, respectively. For f detection, the nanoparticle lies in between the double peak at the zero signal position, and at the main peak maximum

for $2f$. In both cases, the nanoparticle position on the substrate surface is determined with a precision better than the space resolution of the microscope, of the order of d_{FWHM} . This depends on the dynamics of the measurement, and thus on the particle size and incident wavelength, but typical numbers can be estimated to be about 150 nm along the x direction and 50 and 100 nm along the y direction for f and $2f$ detections, respectively.

4.1. Gold nanoparticles

After nanoparticle detection, spectroscopic investigations were performed with polarized or unpolarized light. For most of the investigated particles, on rotating the light polarization direction the measured spectra show two extrema in the spectral position and amplitude of the SPR, corresponding to perpendicular polarization directions (figure 7). This polarization anisotropy suggests a deviation from sphericity of the studied nanoparticles, with an ellipsoidal-like shape, the observed spectra being very similar to those computed for a spheroid (figure 3). Actually, few particles exhibiting more complex light polarization dependent spectra have been detected, suggesting different shape distortion. Their presence in the colloidal solution was also observed in TEM measurements, and they are excluded in the following discussion.

The measurements are only sensitive to the particle shape in the substrate plane and no direct information is obtained in the beam propagation direction (actually information can be extracted from the particle volume determination; see below). To analyse the measured polarization dependent spectra, we have thus assumed that the particles are spheroidal with their short and long main axes in the substrate plane. A prolate shape has been assumed but similar results are obtained for oblate shapes. A very good reproduction of the experimental data is thus obtained (figure 7). This permits one to extract quantitative information on the particle and its orientation on the surface, the observed resonances with extremal wavelengths being associated to polarizations along the short and long axes, respectively. In the fitting procedure, only three parameters were used: a , $\eta = c/a$ and ϵ_m . Actually the particle aspect ratio η is determined by the polarization dependent measurements: the different spectra measured with changing the light polarization are reproduced with the same matrix dielectric constant (ϵ_m) and particle volume (V , or equivalently a). η can thus be precisely determined as well as a and ϵ_m , from the absolute amplitude of the measured σ_a and SPR wavelength. This gives, for the four optically characterized nanoparticles of figure 7, a major axis $2a = 18.5$ nm (a), 19 nm (b), 20 nm (c) and 23 nm (d), with an aspect ratio $\eta = 0.85$ (a) and $\eta = 0.9$ (b), (c), (d). These polarization dependent measurements, associated to a model describing the shape dependence of the optical response of a metal nanoparticle, thus permit one to extract the absolute size, shape and surface orientation of the studied particle.

The only other way to extract such information is by using transmission electron microscopy. In both techniques, only the in-plane projection of the particle shape is accessed. As a comparison of the extracted information cannot be done on a single particle, we have performed measurements on a large

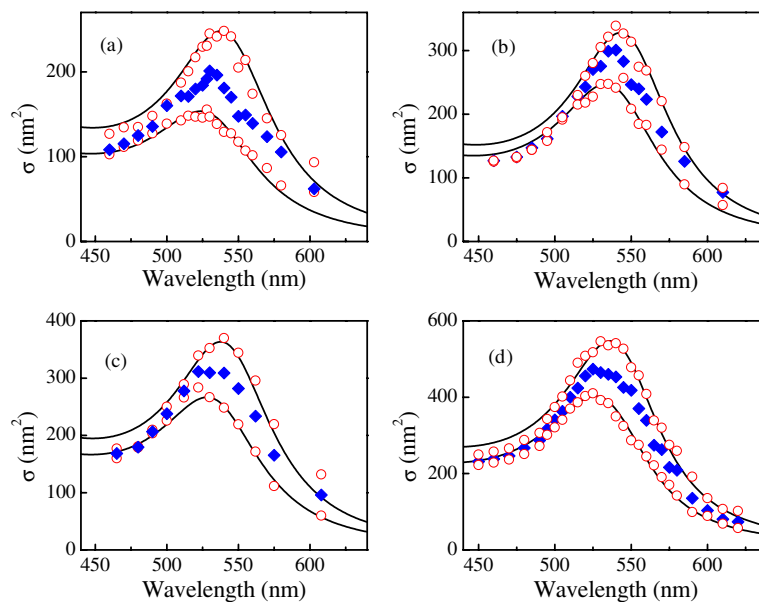


Figure 7. Light polarization dependent spectra of four gold nanoparticles spin-coated on a glass substrate in the presence of PVOH. The open dots show the spectra measured for the two perpendicular light polarization directions corresponding to the maximum and minimum value of the SPR wavelength, and concomitant extrema of the signal amplitude. The diamonds correspond to the unpolarized light spectra. The full lines are theoretical fits assuming elliptical prolate shape nanoparticles, with different parameters described in the text (equation (5)).

number of particles and compared the obtained statistics. The optically deduced statistical distribution of the nanoparticle ellipticity is in excellent agreement with that obtained with TEM measurements. In particular, the same mean ellipticity $\langle \eta \rangle = 0.90$ is found, and similar distributions are observed. Comparable results were obtained in the presence or in the absence of polymer, showing that environment effects do not influence the obtained data.

Though precise determination of the volume of a particle requires fitting of its polarized spectra, in the case of gold a very good estimate can be obtained (for small sphericity deviation) using its unpolarized spectra. This is based on the fact that the unpolarized spectrum is very close to that of a sphere of the same volume, the difference in σ_a amplitude yielding a volume error of about 5% for $\eta = 0.9$ (figure 3). Replacing the real particle by an equivalent sphere, an effective diameter D can thus be extracted by fitting the unpolarized absorption spectra using equation (1). Note that to check the validity of the quasi-static approximation, multipolar expansion of the Mie theory has also been used to fit the data. In this fitting procedure, the only parameters are the particle diameter and local environment dielectric constant. They can be precisely extracted from the measured σ_a amplitude and spectrum (section 2.1).

As for ellipticity, the optically determined statistics of the effective particle diameter D , performed over 43 gold nanoparticles, compares very well with the TEM results [18]. The determined mean particle sizes are consistent, $\langle D \rangle \approx 16.6$ and 16.2 nm, respectively, differing by only 3%, with a standard deviation of 1.1 nm for both distributions. As discussed in section 2.1, the bulk values of the metal dielectric function determined by Johnson and Christy [26] have been used in the fitting procedure after introducing a surface correction. Using the bulk ϵ values compiled by

Palik [30] yields a very similar size distribution with a slight systematic decrease of the extracted diameter of less than 1 nm. The results are still consistent with the TEM data. This agreement, together with that obtained for ellipticity measurements, validates our approach and confirms that the intrinsic geometrical properties of the nanoparticles can be obtained with our optical technique.

The dielectric constant ϵ_m of the local environment of a particle is also obtained from the above analysis. For the samples investigated here, formed by spin-coated particles in air or embedded in a polymer, large variations of ϵ_m have been demonstrated, over a range of $\Delta\epsilon_m \approx 0.5$, around different mean values for the two types of sample (about 2.1 and 1.8, respectively). These results give direct experimental evidence for fluctuations of the local environment on a nanometric scale within the same composite medium. They demonstrate the possibility of using embedded nanoabsorbers as probes of their nanoenvironment, with a potential sensitivity to both the real and imaginary parts of the local environment index on a nanoscale.

4.2. Silver nanoparticles

Similar measurements were performed for silver nanoparticles with a mean diameter of 30 nm. The spectrum measured around the surface plasmon resonance of a single silver particle deposited on a glass substrate and embedded in PVOH is shown in figure 8, together with the normalized absorption spectrum of the initial colloidal solution. The single particle spectrum clearly shows a red shift of the surface plasmon resonance wavelength, consistent with increase of the dielectric constant of its environment (figure 1(b)). An important narrowing of the line is observed by almost a factor of 2 (about 65 nm, as compared to about 30 nm), indicating

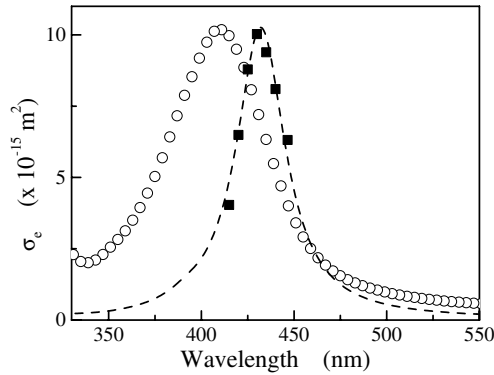


Figure 8. Measured extinction cross-section $\sigma_e \approx \sigma_a$ spectrum of a single silver nanoparticle of 31 nm diameter deposited on a glass substrate in the presence of PVOH (squares). The dashed line is the computed spectra using multipolar expansion of the Mie theory. The open dots are the measured absorption spectrum of the initial colloidal solution normalized to the single particle σ_a peak value.

a strong inhomogeneous broadening of the SPR in ensemble measurements in the colloidal solution.

Actually, in ensemble measurements, each nanoparticle contributes to the signal with its own characteristics, i.e., size, ellipticity and environment, that fluctuate from particle to particle. The material absorption coefficient α is the sum in a unit volume of the individual particle contributions. In the ideal case of perfectly spherical identical particles in an homogeneous environment, the material absorption is simply given by the individual absorption cross-section σ_{abs}^s times the nanosphere density N . Introducing size dispersion in the case of nanospheres only leads to fluctuations of the SPR width via the D dependence of ϵ (equations (3) and (4)), its wavelength being fixed (equation (6) and figure 2). More realistic samples also exhibit particle shape dispersion and environment fluctuations that both introduce fluctuations of the surface plasmon resonance frequency, i.e., inhomogeneous broadening of the SPR. For instance, approximating the particle by nanoellipsoids, the absorption coefficient of a nanomaterial formed by randomly oriented identical nanoellipsoids is obtained by averaging the absorption cross-section over the orientation:

$$\alpha = \frac{N}{3} \sum_{i=x,y,z} \sigma_a^i \quad (11)$$

the polarization dependence being of course lost. In silver, the large sensitivity of the SPR resonance wavelength on the dielectric environment and shape of the nanoparticle, together with its narrow width (figures 1 and 3), are at the origin of the large impact of these fluctuation effects on the SPR width in ensemble measurements. These effects are less noticeable in the case of gold for which the SPR is wavelength stabilized and broadened due to its overlap with the interband transitions. As in gold, fitting of the measured spectrum brings information on the particle size, yielding a particle diameter of about 31 nm.

5. Conclusions

The polarized optical absorption spectra of a single metal nanoparticle contain much information about its geometry

and environment that can be extracted by comparing the computed and experimental spectra, provided that they can be quantitatively measured. This can be done using combination of the recently demonstrated spatial-modulation far-field optical technique with a frequency tunable light source. This approach permits optical identification of a single particle, i.e., determination of its properties: size, shape and orientation. The statistics of the results are in excellent agreement with the TEM data, confirming the validity of our approach. This opens new perspectives for identification and quantitative characterization of a metallic, or more generally, absorbing single nanoobject via its optical signature. In particular, the approach described here for quasi-spherical gold and silver nanoparticles can readily be extended to more complex shapes such as nanorods and nanotriangles.

The possibility of performing *in situ* optical characterization of a single nanoparticle opens up many perspectives for the investigation of the properties of a single nanoobject and their correlation with its geometry and environment. In particular, it is very interesting in sample configurations where electron microscopy cannot be used, such as for nanoparticles embedded in a dielectric matrix. It constitutes an important step forward for the analysis of single nanoparticle properties, using non-linear optical spectroscopy or other non-optical techniques. *In situ* identification of single metal nanoparticles is also important for their further use as optical nanoprobe of their local environment on a nanometre scale, avoiding the averaging effect inherent to ensemble spectroscopy.

References

- [1] Kreibig U and Vollmer M 1995 *Optical Properties of Metal Clusters* (Berlin: Springer)
- [2] Bohren C F and Huffman D R 1998 *Absorption and Scattering of Light by Small Particles* (New-York: Wiley)
- [3] Voisin C, Del Fatti N, Christofilos D and Vallée F 2001 *J. Phys. Chem. B* **105** 2264
- [4] Link S and El-Sayed M A 1999 *J. Phys. Chem. B* **103** 8410
- [5] McFarland A D and Van Duyne R P 2003 *Nano Lett.* **3** 1057
- [6] Mock J J, Smith D R and Schultz S 2003 *Nano Lett.* **3** 485
- [7] Soennichsen C, Franzl T, Wilk T, von Plessen G and Feldmann J 2002 *New J. Phys.* **4** 93.1
- [8] Klar T, Perner M, Grosse S, Von Plessen G, Spirkel W and Feldmann J 1998 *Phys. Rev. Lett.* **80** 4249
- [9] Mikhailovsky A A, Petruska M A, Stockman M I and Klimov V I 2003 *Opt. Lett.* **28** 1686
- [10] Liu A, Rahmani A, Bryant G W, Richter L J and Stranick S J 2001 *J. Opt. Soc. Am. A* **18** 704
- [11] Moerner W E and Orrit M 1999 *Science* **283** 1670
- [12] Empedocles S A, Norris D J and Bawendi M G 1996 *Phys. Rev. Lett.* **77** 3873
- [13] Hartschuh A, Pedrosa H N, Novotny L and Krauss T D 2003 *Science* **301** 1354
- [14] Lindfors K, Kalkbrenner T, Stoller P and Sandoghdar V 2004 *Phys. Rev. Lett.* **93** 37401
- [15] Kalkbrenner T, Håkanson U and Sandoghdar V 2004 *Nano Lett.* **4** 2309
- [16] Boyer D, Tamarat P, Maali A, Lounis B and Orrit M 2002 *Science* **297** 1160
- [17] Arbouet A, Christofilos D, Del Fatti N, Vallée F, Huntzinger J R, Arnaud L, Billaud P and Broyer M 2004 *Phys. Rev. Lett.* **93** 127401
- [18] Muskens O L, Del Fatti N, Vallée F, Huntzinger J R, Billaud P and Broyer M 2006 *Appl. Phys. Lett.* at press
- [19] Mie G 1908 *Ann. Phys., Lpz.* **25** 377
- [20] Kawabata A and Kubo R J 1966 *J. Phys. Soc. Japan* **21** 1765

- [21] Flytzanis Ch, Hache F, Klein M C, Ricard D and Roussignol Ph 1991 *Progress in Optics* vol XXIX, ed E Wold (Amsterdam: North-Holland) p 321
- [22] Vallée F, Del Fatti N and Flytzanis Ch 1997 *Nanostructured Materials* ed V M Shalaev and M Moskovits (Washington, DC: American Chemical Society) p 70
- [23] Hache F, Ricard D and Flytzanis Ch 1986 *J. Opt. Soc. Am. B* **3** 1647
- [24] Voisin C, Christofilos D, Del Fatti N, Vallée F, Prével B, Cottancin E, Lermé J, Pellarin M and Broyer M 2000 *Phys. Rev. Lett.* **85** 2200
- [25] Arbouet A *et al* 2003 *Phys. Rev. Lett.* **90** 177401
- [26] Johnson P B and Christy R W 1972 *Phys. Rev. B* **6** 4370
- [27] Lermé J, Palpant B, Prével B, Pellarin M, Treilleux M, Vialle J L, Perez A and Broyer M 1998 *Phys. Rev. Lett.* **80** 5105
- [28] Haes A J, Zou S, Schatz G C and Van Duyne R P 2004 *J. Phys. Chem. B* **108** 6961
- [29] Del Fatti N, Muskens O, Christofilos D and Vallée F 2005 *Proc. SPIE* **5725** 318
- [30] Palik E D 1985 *Handbook of Optical Constants of Solids* vol I (New York: Academic)
- Palik E D 1991 *Handbook of Optical Constants of Solids* vol II (New York: Academic)